A 3D Chebyshev-Fourier algorithm for convection equations in low Mach number approximation

Ouafa Bouloumou* — Eric Serre* — Jochen Fröhlich**

** MSNM-GP UMR 6181*
38 rue F. Joliot-Curie, 13451 Marseille cedex 20, France
ouafa.bouloumou@l3m.univ-mrs.fr

*** Institute for Fluid Mechanics, Technical University of Dresden*
01062 Dresden, Germany

ABSTRACT. *A three-dimensional spectral method based on Chebyshev-Chebyshev-Fourier discretizations is presented in the framework of the low Mach number approximation of Navier-Stokes equations. The working fluid is assumed to be a perfect gas with constant thermodynamic properties. The generalized Stokes problem, which arises from the time discretization by a second-order semi-implicit scheme, is solved by a preconditioned iterative Uzawa algorithm. Several validation results are presented in the case of steady and unsteady flows. This model is also evaluated for natural convection flows with large density variations in the case of a tall differentially heated cavity of aspect ratio 8. It is found that on contrary to convection at small temperature differences (Boussinesq), the 2D unsteady solution at Ra =* 3.4×10^5 *is unstable to 3D perturbations.*

RÉSUMÉ. *Dans ce travail nous présentons une méthode numérique basée sur une approximation spectrale Chebyshev-Chebyshev-Fourier des équations de la convection dans le cas de fortes variations de densité au moyen d'un modèle faible nombre de Mach. Le problème de Stokes issu de la discrétisation temporelle des équations de Navier-Stokes par un schéma semi-implicite du second ordre en temps, est résolu avec un algorithme itératif de type Uzawa préconditionné. Le code est validé sur des résultats de la littérature en régime stationnaire et instationnaire. Le modèle a également été évalué dans le cas d'une cavité différentiellement chauffée allongée de rapport de forme 8. Contrairement au cas Boussinesq, la solution 2D instationnaire à Ra =* 3.4×10^5 *s'est montrée instable par rapport à une perturbation 3D.*

KEYWORDS: *spectral methods, convection, low Mach number.*

MOTS-CLÉS : *méthodes spectrales, convection, faible nombre de Mach.*

DOI:10.3166/EJCM.18.607-625

1. Introduction

Thermal convection in differentially heated enclosures has been of interest since a long time, in order to provide a good scientific understanding and satisfactory quantitative predicted simulations for engineering practices. Solving this problem also allows testing and validating numerical methods since the comparison with experiment results proves often delicate because of the difficulty of carrying out adiabatic boundary conditions (Leong *et al.*, 1998). Most benches of natural convection deal with the Boussinesq approximation (BO) limited to small temperature differences (Gray *et al.*, 1976). Non-Boussinesq effects result from the compressibility and/or the variation of the physical properties with the temperature. In this case, suitable formulations are required. Paolucci (1982) derives a set of acoustic waves filtered equations of parabolic nature similar to the incompressible case for the viscous flows. This so called low Mach number (LMN) approximation authorizes important variations of temperature and allows a better description of the flow.

Spectral methods have been shown to perform extremely well for investigating transition to turbulence in enclosed natural convection flows under the Boussinesq approximation, since they ensure an accurate description of the instability modes, of the thresholds and of the bifurcation under large heat gradients (Roux, 1990). For non-Boussinesq convection, most of the numerical works in enclosed cavity have been limited to the bidimensional spectral approximations due to the numerical difficulties and the inherent cost of the three dimensional computations whereas the third dimension provides a more realistic approximation of regimes covered by convection or transition to the turbulence. In particular, as far as the authors know, only 2D configurations were treated until now using either with Chebyshev/Fourier (Fröhlich *et al.*, 1990) or Chebyshev/Chebyshev (LeQuéré *et al.*, 1992) approximation in LMN context. Three-dimensional cases have been limited to second-(Accary *et al.*, 2006) or fourth-(Nicoud, 2000) order space-accuracy using finite volume and finite difference schemes, respectively. In (Fröhlich *et al.*, 1990), the use of a staggered grid implies repetitive interpolations between the grids, and in (LeQuéré *et al.*, 1992) the derivative operators are tensorial and thus of large size. Consequently, the 3D extension from these previous works was not straightforward.

In the present work, a three-dimensional spectral method has been developed for Cartesian enclosures based on a Chebyshev-Chebyshev-Fourier approximation. The spectral convergence of the error as well as the second-order accuracy in time has been obtained. Benchmark validations have been then performed both in the LMN approximation in the case of steady regime (LeQuéré *et al.*, 2005) and in the Boussinesq limit for unsteady regime (Christon *et al.*, 2002). Finally, transition to 2D and 3D unsteady regimes has been investigated in natural convection flow within tall enclosure of aspect ratio 8.

2. Modelling and problem formulation

A natural convection air flow is considered within a differentially heated cavity depicted in Figure 1, where H is the height, L_y the width and L_x the depth of the enclosure. Aspect ratios of the cavity are defined as $A_y = H/L_y$ and $A_x = L_x/L_y$. The channel of the cavity consists of two horizontal passive adiabatic walls and one homogenous direction; the vertical walls in the y-direction are maintained isothermal at a hot and a cold temperature, T_h and T_c, respectively. The buoyancy force due to the gravity works downwards and the temperature difference $T_h - T_c$ is assumed large enough to frustrate the Boussinesq approximation.

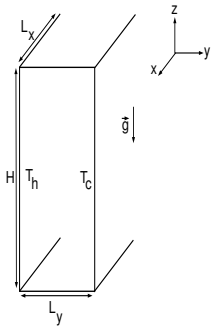

Figure 1. *Geometric description of the cavity problem*

The physical governing equations are those suggested by Paolucci (Paolucci, 1982) describing the flow of a thermally expandable perfect gas under the LMN assumption. All the variables involved in the complete Navier Stokes and the energy equations are expanded in terms of γM^2 powers, $M \ll 1$ being the Mach number flow and γ the ratio of specific heats. Pressure is then split into a thermodynamic spatially homogeneous part, a hydrostatic time-independent part and a dynamic density-decoupled part, allowing the filtering of acoustic waves. The leading of this expansion at lowest order, the set of dimensionless equations written in non-conservative form reads,

$$\partial_t \rho + \nabla.(\rho V) = 0 \quad [1]$$

$$\rho(\partial_t V + V.\nabla V) + \nabla P = \frac{-1}{2\varepsilon Pr}(\rho - 1)e_z + \frac{1}{\sqrt{Ra}}\nabla.\tau \quad [2]$$

$$\rho(\partial_t \theta + V.\nabla\theta) - \frac{\gamma - 1}{\gamma} d_t P_0 = \frac{1}{Pr\sqrt{Ra}}\nabla^2\theta \quad [3]$$

$$\rho = \frac{P_0}{\theta} \quad [4]$$

$$d_t P_0 = \frac{\gamma}{Pr\sqrt{Ra}} \frac{1}{|\Omega|} \int_\Omega \nabla^2\theta d\theta \quad [5]$$

where variables ρ, V, θ and P denote density, velocity, temperature and the dynamic pressure component. $\tau = \mu(\nabla V + (\nabla V)^t - \frac{2}{3}(\nabla.V)I)$ being the viscous stress tensor. The system has been made dimensionless by introducing the reference scaling quantities: $T^* = (T_h + T_c)/2$, $L^* = L_y$, $t^* = L^*/V^*$, $V^* = \sqrt{Ra}\nu^*/L^*$, and $P^* = \rho^* V^{*2}$. with Ra the Rayleigh number given by $Ra = (2\varepsilon g^* L^{*3})/(\nu^*\kappa^*)$ and the relative temperature difference is $\varepsilon = (T_h - T_c)/2T^*$. Boundary conditions for the temperature are $\theta_h = 1 + \varepsilon$, $\theta_c = 1 - \varepsilon$ and $\partial_z\theta(z = \mp H/2) = 0$. No-slip conditions are imposed for the velocity and no boundary conditions are required for the pressure. The viscosity μ and the thermal conductivity κ are taken constant for the moment but Sutherland laws could be considered. The Prandtl number Pr is always fixed to 0.71 and the specific heat ratio is set to 1.4. It is known that the onset of unsteady convection can be influenced by the initial condition (LeQuéré *et al.*, 1992). In this work, an isothermal fluid initially at rest has been considered with or without additional random perturbations that will be specified further.

3. Numerical method

3.1. *Space discretization and time integration*

The spatial approximation method consists of truncated series expansion and tensor product. Each dependent variable $\phi = (V, P, \theta, \rho)$ is developed in a Fourier series with respect to x direction and Chebychev polynomials in the non periodic directions y and z such that:

$$\phi_{KNM}(x, y, z, t) = \sum_{k=-K}^{K} \sum_{n=0}^{N} \sum_{m=0}^{M} \phi_{nm}^{k}(t) T_n(y) T_m(z) e^{(ikx)}$$

where K, N, M are the highest degrees of interpolating polynomials in directions x, y and z, respectively. Spatial discrete equations are obtained using the Fourier Galerkin / Chebychev-collocation method. The usual Gauss-Lobatto points are adopted in both non-homogeneous directions such that $y_j = \cos(\frac{\pi j}{N})$ and $z_i = \cos(\frac{\pi i}{M})$ with $0 \leq i \leq M$ and $0 \leq j \leq N$ for all quantities, except the pressure , which is calculated within the domain only. A $P_N - P_{N-2}$ formulation is used to satisfy the inf-sup condition of the Stokes problem and thus avoid spurious pressure modes (Maday *et al.*, 1992). Consequently, no staggered grid is needed.

The time integration is carried out with a second-order semi-implicit scheme, corresponding to a combination of the second-order backward differentiation formula for the viscous diffusion term and the Adams-Bashforth scheme for the nonlinear terms (Vanel *et al.*, 1986) and reads for the above equations,

$$\frac{3\phi^{n+1} - 4\phi^n + \phi^{n-1}}{2\delta t} + \mathcal{L}(\phi^{n+1}) = 2\mathcal{M}(\phi^n) - \mathcal{M}(\phi^{n-1})$$

where $\mathcal{L}$ and $\mathcal{M}$ denote linear and non-linear operators respectively, and $\phi = (V, \theta)$. Unlike the Boussinesq approximation, the non-linearities are not only confined in the

convective term, but also in the density and in the eventual physical properties variations, which provide additional nonlinearities in the LMN model. As suggested by Gottlieb *et al.* (1977) the diffusion term is treated explicitly, and a stabilizing term is added on both sides of the equation that is treated implicitly on the left-hand side and explicitly in the right-hand side. An optimal choice of this stabilizing term might be as close as possible to the most active part of the diffusion term in order to capture its largest variation. Then, in order to obtain linear and time independent operators and in order to transfer algebraic cost into pre-processing, we introduce a density decomposition into two parts, as initially proposed in 2D by Fröhlich *et al.* (1990) such that,

$$\rho(x,y,z,t) = \rho_s(y,z) + (\rho(x,y,z,t) - \rho_s(y,z)) \qquad [6]$$

Multiplying all transport equations by a factor $\rho_s/\rho = O(1)$ allows us to balance the density fluctuations in the source term and inhibits the coupling of Fourier modes and the time variation of density.

3.2. *Energy equation*

Thanks to semi-implicit discretization and density-pressure decoupling, one can calculate density field at time level $(n+1)$ by integrating the energy equation and by using the equation of state before solving the dynamic field. For instance, the previous procedure applied to energy equation yields:

$$(\sigma\rho_s - \nabla^2)\theta^{n+1} = F_\theta \qquad [7]$$

$$F_\theta = \{\frac{\rho_s}{\rho}\frac{\gamma-1}{\gamma}d_t P_0 - \rho_s V.\nabla\theta + (\frac{\rho_s}{\rho}-1)\frac{1}{Pr\sqrt{Ra}}\nabla^2\theta\}^{n,n-1} + \frac{\sigma}{3}\rho_s(4\theta^n - \theta^{n-1})$$

where $\{\phi\}^{n,n-1} = 2\phi^n - \phi^{n-1}$ and $\sigma = \frac{3}{2\delta t}$, with δt the time step. Consequently, the temperature is obtained by solving the linear Helmholtz problem [7]. However, because of tensor products, the matrix size grows like N^4 for each Fourier mode precluding an explicit construction of the operator. Indeed, in our configuration, the principal temperature variations occur in a privileged direction, thus it is convenient to split the density $\rho_s(y,z)$ into $\rho_s(y) + \rho_s(z)$ and to recourse to diagonalization techniques (Haidvogel *et al.*, 1979), since the equation is henceforth simplified as $A\phi + \phi B^t = F_\theta$.

3.3. *Density and thermodynamic pressure*

From θ^{n+1}, the density ρ^{n+1} is obtained by Equation [4], which however requires the knowledge of P_0^{n+1}. In the present case, the cavity is closed. The boundary

conditions applied for the velocity impose constant mass inside the computational domain Ω. The total mass at each instant $M = const.$ hence is equal to its initial value which is calculated from a reference temperature field and a reference value for the thermodynamic pressure. Then, the thermodynamic pressure is given by

$$P_0^{n+1} = \frac{M}{\int_\Omega \frac{1}{\theta^{n+1}} d\Omega} \qquad [8]$$

For the reference state the purely conducting state has been chosen. For constant conductivity this yields a linear temperature distribution. The thermodynamic pressure is given by

$$P_0 = 2\varepsilon / ln(\frac{1+\varepsilon}{1-\varepsilon}) \qquad [9]$$

Taking into account the energy Equation [3], the mass conservation equation can be written as

$$\nabla.V = \frac{1}{P_0}(\frac{1}{Pr\sqrt{Ra}}\nabla^2\theta - \frac{1}{\gamma}d_t P_0) \qquad [10]$$

Consequently, time variations of P_0 must ensure compatibility with boundary conditions of velocity. Integrating Equation [10] and imposing the present boundary conditions yields Equation [5]. For reasons of compatibility $d_t P_0$ must be determined from this equation rather than, e.g., from a finite difference employing $P_0^{n+1}, P_0^n, P_0^{n-1}$ as shown in (Fröhlich *et al.*, 1990). This is applied in the present algorithm.

3.4. *Stokes problem*

The time discretization of motion equations, combined to a similar technique as in the energy equation, leads to the following Stokes problem at time level $(n+1)$:

$$\mathcal{L}V^{n+1} + \frac{\rho_s}{\rho^{n+1}}\nabla P^{n+1} = F_V \qquad [11]$$

$$\nabla.V^{n+1} = F_R \qquad [12]$$

where $\mathcal{L}$ is the velocity Helmholtz operator. The source terms F_V and F_R made of previous velocity time extrapolation and of the known following quantities ρ^{n+1}, θ^{n+1} and $d_t P_0^{n+1}$, write as

$$\begin{aligned} F_V = &\{-\rho_s V.\nabla V + \frac{1}{\sqrt{Ra}}(\frac{\rho_s}{\rho}\nabla.\tau - \widetilde{\nabla}^2 V)\}^{n,n-1} \\ &+ \frac{\sigma}{3}\rho_s(4V^n - V^{n-1}) + \frac{\rho_s}{\rho^{n+1}}\frac{-1}{2\varepsilon Pr}(\rho^{n+1} - 1)e_z \end{aligned} \qquad [13]$$

$$F_R = \frac{1}{P_0}(\frac{-1}{\gamma} d_t P_0 + \frac{1}{Pr\sqrt{Ra}}\nabla^2\theta) \quad [14]$$

with

$$\widetilde{\nabla}^2 = \begin{pmatrix} \frac{4}{3}\partial_{xx} + \partial_{yy} + \partial_{zz} & 0 & 0 \\ 0 & \partial_{xx} + \frac{4}{3}\partial_{yy} + \partial_{zz} & 0 \\ 0 & 0 & \partial_{xx} + +\partial_{yy} + \frac{4}{3}\partial_{zz} \end{pmatrix}$$

With appropriate velocity boundary conditions, an expression of the velocity field is obtained from Equation [11] by inverting the operator $\mathcal{L}$. Then, using this expression in the continuity Equation [12], we obtain Equation [15]

$$\nabla.V = -\nabla.\mathcal{L}^{-1}(\frac{\rho_s}{\rho}\nabla P) + \nabla.\mathcal{L}^{-1}F_V \quad [15]$$

It must be notice that the operator $\mathcal{L}$ is inverted once during the pre-processing. Equation [15] is a linear equation for the pressure field that, by omitting time indexes, reads

$$\mathcal{A}(P) = F \quad [16]$$

The so called Uzawa operator is then defined by

$$\mathcal{A} = \nabla.\mathcal{L}^{-1}(\frac{\rho_s}{\rho}\nabla)$$

and

$$F = -F_R + \nabla.\mathcal{L}^{-1}F_V$$

The Uzawa's iterative method solves at each time step the steady problem [16] and does not refer to any time sub-stepping. Nevertheless, the pressure operator is bad-conditionned and requires preconditionning in order to improve the performances of the method. As shown by Fröhlich *et al.* (1992) the use of a fully implicit scheme for the pressure is highly recommended for stability reasons when large departures from the Boussinesq regimes have to be considered. The operator $\widetilde{\mathcal{A}} = \nabla.\mathcal{L}^{-1}(\nabla)$ has been chosen as preconditionner since it is close to $\mathcal{A}$ because $\rho_s/\rho = o(1)$. Gauthier (1988) showed that the convergence rate obtained with this preconditionner is satisfying. Due to the asymmetric and non definite nature of this large matrix $\mathcal{A}$, a PCR (for Precondionned Conjugate Residual) algorithm was chosen for the resolution of the Uzawa equation

3.5. *Memory and preconditioning*

In theory, the best approach would be to calculate and to store $\widetilde{\mathcal{A}}^{-1}$ at the beginning of the simulation once and for all. In practice this explicit construction is prohibitively large. In Due to the Fourier expansion in one direction the matrices were one-dimensional and hence of reasonable size in (Fröhlich *et al.*, 1990). In (LeQuéré *et al.*, 1992), derivative operators were much larger because of tensor product of the

two Chebyshev directions. Memory requirements quickly become excessive in the 3D case. Hence, a direct approach is possible only when dealing with relatively few degrees of freedom, the memory depending on the mesh is shown in Figure 2. Despite the sparse nature of the Helmholtz operators, the assembling the operator $\mathcal{A}$ leads to a full matrix. Technics for sparse matrices can hence not be employed. Dynamic allocation of memory for all the matrices only temporarly used was tested but reduced memory requirements only by a factor of about 4 with a $64\times49\times49$-grid. A sequential reading from a file of matrice elements already calculated is even more time consuming because of the data transfer. The iterative alternative seems therefore to be the best way to avoid explicit matrix construction. Below $N = 32$, there is no noticable difference in memory consumption and the two approaches seem equivalent. Beyond $N = 40$, the difference quickly becomes exponential showing the disadvantage of a direct inversion (Figure 2). indeed, with the Conjugate Residual (CR) algorithm, a considerable gain in memory requirement was obtained even for a small grids, e.g. 95.8% for $N = 48$. On the other hand, the direct approach turned out to be more accurate and faster (no internal iterations), and was then preconized in the present paper with the considered meshes. in this case, $3 \times 10^{-3}s$ (for each mode) was needed in the preprocessing and $2.33 \times 10^{-6}s$ for one global iteration. Uzawa iterations don't exceed 6 while the iterative algorithm required at most 10 internal iterations in each Uzawa iteration. One global iteration consume $1.6 \times 10^{-4}s$ and the preprocessing time is of $1.07 \times 10^{-5}s$.

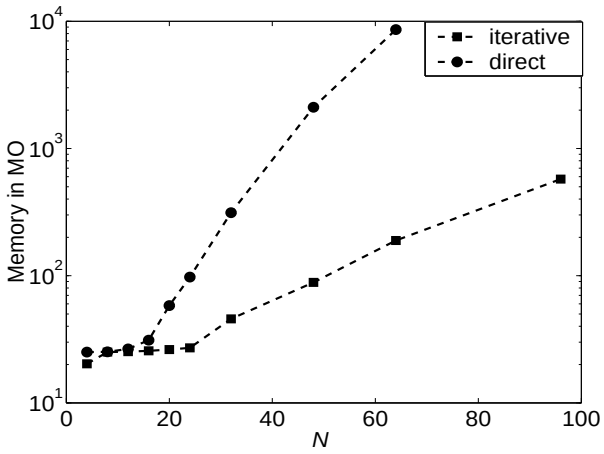

Figure 2. *Evolution of the memory consumption with grid resolution*

3.6. *Time marching procedure*

Assuming the flow is known up to time level (n), the time level $(n+1)$ is obtained by the iterative way described here after,

– Computation of F_θ and of θ^{n+1},

– Computation of the thermodynamic pressure and its time derivative,

– Computation of the density through the state equation,

– Computation of the velocity field divergence F_R,

– Computation of F_V,

– vi. Computation of the pressure and velocity field by resolving the generalized Stokes problem using the PCR algorithm.

4. Validation

4.1. *Space and time accuracy: analytical solution*

The space and time accuracy have been checked using the analytical solution given by Equations [17-22]. It should be noticed here that the thermodynamic pressure is considered constant for simplicity reasons, but that the velocity field is not divergence free and density variations are considered. The solution is

$$u_a = (1+\beta\cos^2\pi t)\frac{1}{2}\sin^2 x\sin 2\pi y\sin 2\pi z \qquad [17]$$

$$v_a = (1+\beta\cos^2\pi t)\frac{1}{4}\sin 2x\sin^2\pi y\sin 2\pi z \qquad [18]$$

$$w_a = (1+\beta\cos^2\pi t)\frac{-1}{2}\sin 2x\sin 2\pi y\sin^2\pi z \qquad [19]$$

$$P_a = (1+\beta\cos^2\pi t)\cos x\cos\pi y\cos\pi z \qquad [20]$$

$$\rho_a = (1+\beta\cos^2\pi t)[\rho_s(y,z) + (\frac{-1}{2}+\frac{1-\sin x}{2-\cos x})\cos\frac{\pi}{2}y\cos\frac{\pi}{2}z] \qquad [21]$$

$$\theta_a = \frac{1}{\rho_a} \qquad [22]$$

where β is a parameter equal to zero or one. From this exact solution, appropriate forcing terms and boundary conditions are deduced. The tests reported here were performed with $Ra = 10^3$ and $\varepsilon = 0.3$.

4.2. *A steady state solution ($\beta = 0$)*

The space accuracy is evaluated using the $\mathcal{L}_2$-errors between the exact and the numerical solution. Steady solution is supposed to be reached when,

$$\left\|\phi^{n+1} - \phi^n\right\|_\infty \approx 10^{-10}$$

Tests have been carried out for $9 \leq N \leq 57$ in each direction. Errors in Figure 3 illustrate the typical exponential behaviour of spectral methods. For the temperature

and the three velocity components, the spectral convergence is obtained and the errors decay to finally reach the zero-machine. The exact solution is well represented from $N = 32$. Note that the pressure error remains small but it is however slightly larger than for the other variables, because the pressure resolution is related to an iterative procedure with a convergence criterion of 10^{-6}. The slight stagnation of the errors from $N = 50$ is a classic phenomenon resulting from round-off error.

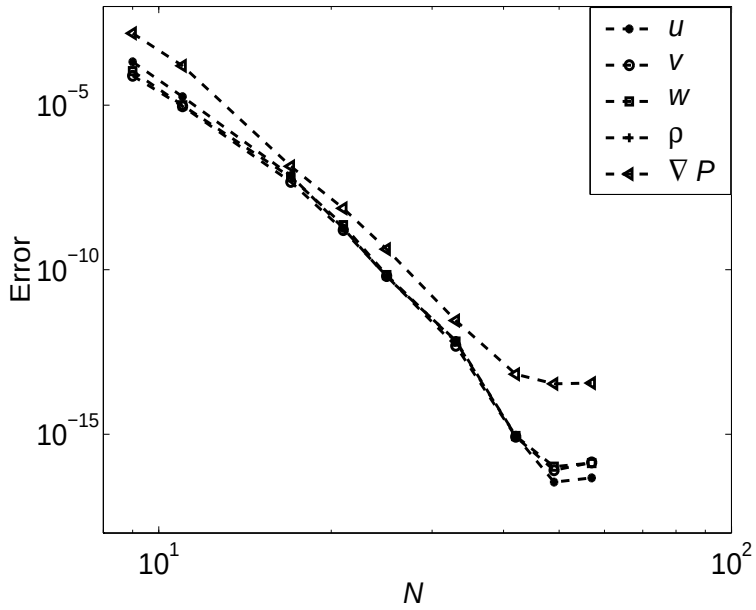

Figure 3. *Space accuracy for a 3D steady exact solution. Evolution of $\mathcal{L}_2$-errors for the velocity, the temperature and the pressure versus the polynomials degree N*

4.3. *Unsteady solution ($\beta = 1$)*

The analytical solution is 2-periodic. The time evolution of the $\mathcal{L}_2$-errors (23) is shown in Figure 4 for various time steps and points in each direction. We evaluate the time accuracy of the scheme on the exact solution with $\beta = 1$ which is 2-periodic. Various time steps are considered for a grid with $N = 24$. Figure 4 shows the time evolution of the errors

$$E(t, \delta t) = \left\| \phi_N^{n+1} - \phi_a \right\|_2 \qquad [23]$$

After a transient time, the errors oscillate around a value which decreases with the time step from around 10^{-4} to 10^{-9}. The computations show the stability of the

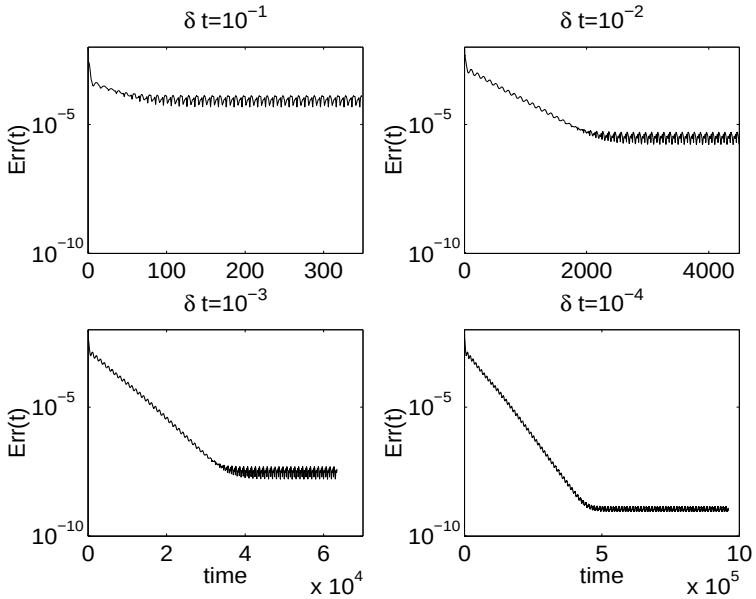

Figure 4. *Time evolution of the $\mathcal{L}_2$-error of the v-velocity for a 3D unsteady exact solution for several time steps and $N = 24$*

numerical solution over time. Figure 5 shows the second order time accuracy of the scheme for all variables. It represents the largest time error defined by

$$E(t) = \max_t E(t, \delta t)$$

where the maximum in time is estimated when the periodic state is reached. For the smallest δt, the errors saturate due to the spatial errors accumulation over time.

4.4. *Benchmark Tests*

The method is evaluated by calculating laminar steady and unsteady natural convection benchmark problems both within a square and within a 8:1 tall cavity. All the computations are two-dimensional. The calculated data have been the thermodynamic pressure together with the averaged Nusselt number. Following results are made dimensionless following the references (LeQuéré *et al.*, 2005) and (Christon *et al.*, 2002). Two grid tests have been carried out for completeness.

4.4.1. LMN benchmark

The two-dimensional steady benchmark test in a square cavity (LeQuéré *et al.*, 2005) has been firstly considered, restricted to the case of constant thermodynamic

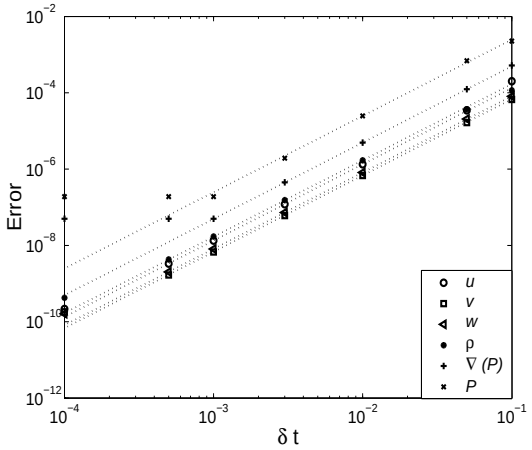

Figure 5. *Time accuracy of the algorithm. Evolution of the $\mathcal{L}_2$-errors of variables versus the time step for an unsteady exact solution and $N = 24$*

Table 1. *Comparison of characteristic quantities for the differentially heated air-filled square cavity LMN-benchmark problem at $\varepsilon = 0.6$ and constant thermodynamic properties*

	$Ra = 10^5$		$Ra = 10^6$	
	Nu	P_0^n	Nu	P_0^n
$N = 48$	4.5513	0.85180	8.220	0.85570
$N = 80$	4.5517	0.85177	8.85977	0.85637
(Accary *et al.*, 2006) $N = 120$	4.5542	0.85181	8.8581	0.85685
(Becker *et al.*, 2002) $N = 2050$	–	–	8.8597	0.85634
(Heuveline, 2003) $N = 925$	–	–	8.8598	0.85634
(Paillere *et al.*, 2000) $N = 160$	4.5631	0.85160	–	–
(LeQuéré *et al.*, 2005) reference	–	–	8.85978	0.856338

properties of the fluid and for $Ra = 10^6$. Additional calculations have been performed for $Ra = 10^5$. For both values of Rayleigh number, the agreement with the literature is very good as shown in Table 4.4.1. Calculations have been assumed to be converged at the same digits of reference solutions. The structure of the flows is not shown here but it is completely similar to those obtained by (Paillere *et al.*, 2000).

4.4.2. BO limit

The BO limit of the LMN code has been investigated in the oscillatory regime of convection within the 8:1 tall cavity (Christon *et al.*, 2002). Computations have been

Table 2. *Data at point-1* $(y = 0.181, z = 7.370)$ *inside a 8:1 cavity benchmark problem (Christon et al., 2002) in the BO approximation. For each quantity and from top to bottom: current results with* $N = 25 \times 91$*, Guo et al. (2002) with a grid* $N = 40 \times 120$ *and Xin et al. (2002) with a grid* $N = 48 \times 180$

Quantity	Average	Amplitude	period
v_1	0.056000	0.053900	3.4120
	0.056110	0.052940	3.4220
	0.056356	0.054829	3.4115
w_1	0.46382	0.075800	3.4120
	0.46200	0.075120	3.4220
	0.46188	0.077206	3.4115
θ_1	0.26500	0.040000	3.4120
	0.26540	0.041340	3.4250
	0.26548	0.042735	3.4115
Nu^h	4.58000	0.69230×10^{-2}	3.4305
	4.57950	0.68920×10^{-2}	3.4220
	4.57946	0.71000×10^{-2}	3.4115
Nu^c	4.58000	0.69230×10^{-2}	3.4305
	4.57950	0.68900×10^{-2}	3.4220
	4.57946	0.70995×10^{-2}	3.4115

performed for $Ra = 3.4 \times 10^5$, $\varepsilon = 0.01$, in the case of a perfect gas with constant transport coefficients μ and κ. The grid used here is a 25×91-mesh in both (y, z) directions. All the data are reported in Table 4.4.2 and show a very good agreement with the reference results of Xin *et al.* (2002). Indeed, the solution is oscillatory with a period of around 3.42, similar to the one obtained in BO results. The Nusselt number, the average values of the flow field variables as well as their amplitudes are also very close to the ones obtained by Xin *et al.* (2002). Moreover, heat transfer distributions are symmetrical on the hot and cold walls as expected in the BO case.

5. Results

The ability of the numerical method to deal with 2D and 3D natural convection problems with large temperature difference $\varepsilon = 0.6$ (non-Boussinesq convection) is shown in this section. The stability of a two-dimensional low Mach number solution with respect to 3D perturbations in the x-direction has been investigated at a supercritical Rayleigh number and within a tall cavity of aspect ratios $A_y = 8$ and $A_x = 2.017$. There is noticeable difference between two- and three-dimensional results according to Saeid *et al.* (2005) where differential heating and species concentration were investigated. It was found that free surface yields higher rate of heat and mass transfer. The

effect of lateral aspect ratio on the heat, mass, and momentum transfer was examined in (Mohamad *et al.*, 2004) in the frame work of a binary fluid filled cavity.

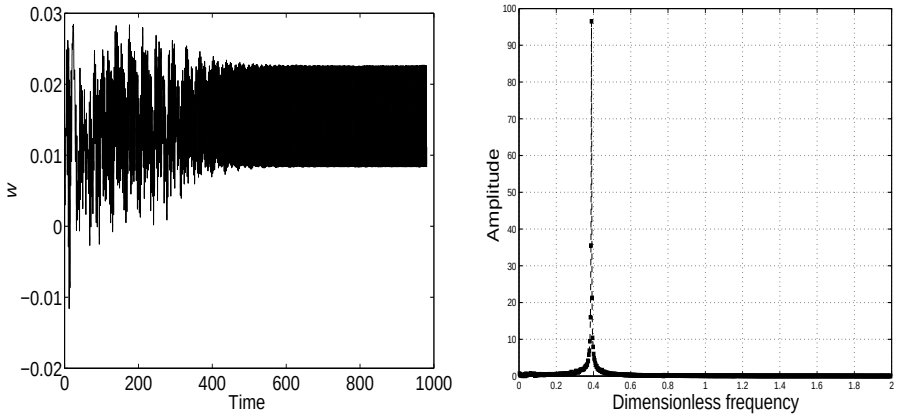

(a) (b)

Figure 6. *w-velocity at $Ra = 3.4 \times 10^5$ in 2D case, (a) Time history and (b) Spectrum frequency of asymptotic solution*

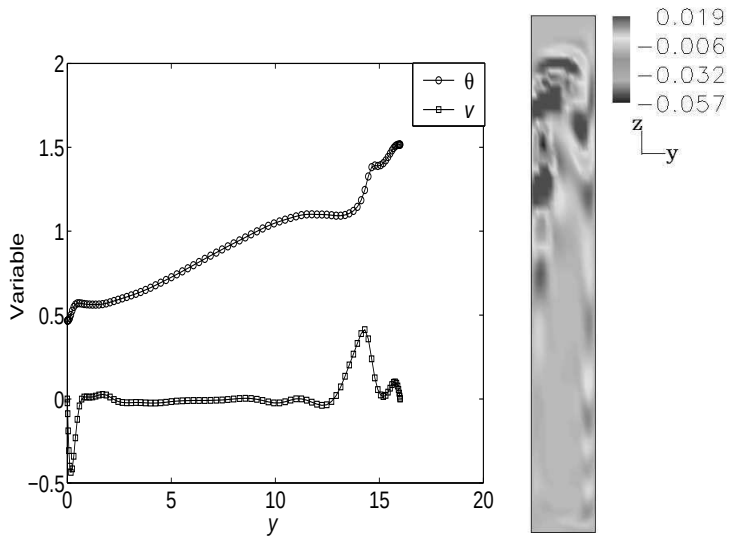

(a) (b)

Figure 7. *2D natural convection in LMN approximation at $Ra = 3.4 \times 10^5$. (a) Horizontal profiles in the y-direction at half cavity height of the temperature and the velocity, (b) Fluctuating temperature field in the (y, z) plan*

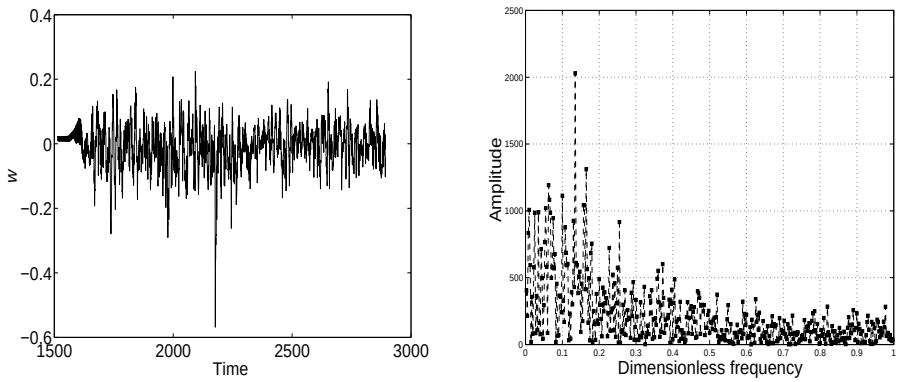

(a) (b)

Figure 8. *Temporal behaviour of the solution in the 3D case at* $Ra = 3.4 \times 10^5$. *(a) Time evolution of the* w*-velocity component at the cavity centre, (b) Power spectrum of the* w*-velocity*

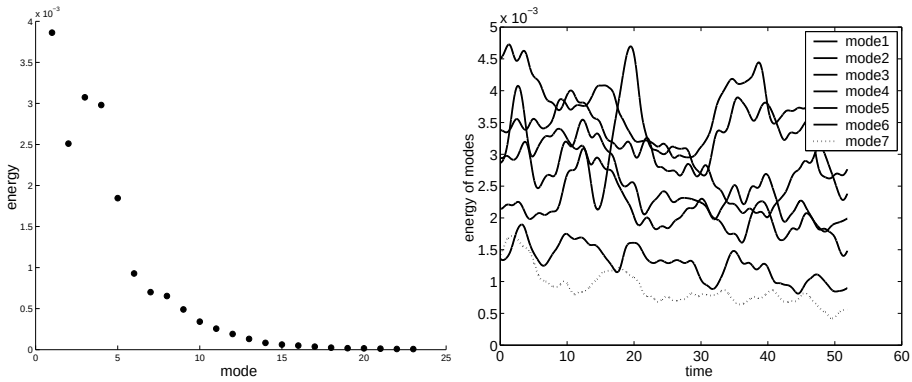

(a) (b)

Figure 9. *3D natural convection at* $Ra = 3.4 \times 10^5$ *using the LMN approximation. (a) Instantaneous Fourier spectrum in space of the kinetic energy at t=15, (b) Time evolution of the energy of the Fourier-modes* $k = 1 \ldots 8$

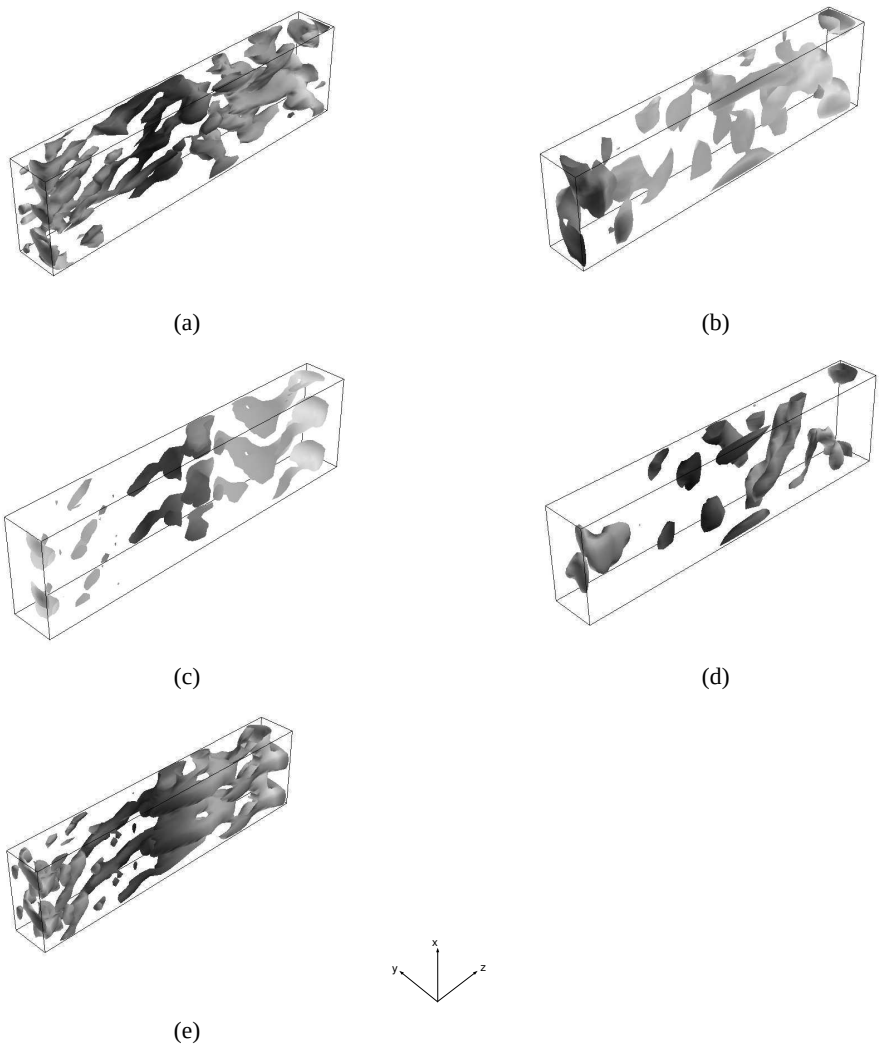

Figure 10. *3D natural convection at $Ra = 3.4 \times 10^5$ using the LMN approximation. (a) Iso-surfaces of the U-component of the velocity. (b,c) Isosurface of the modes 1 and 2 of U, respectively. (d,e) Isosurface of the modes 1 and 2 of the fluctuating U, respectively*

Firstly, a 2D cavity has been considered with a mesh of 25×91 grid points in both (y, z) directions. Increasing step by step the Rayleigh number, an oscillatory two-dimensional solution of period 2.8 is obtained at a critical Rayleigh number evaluated between 2.8×10^5 and 2.9×10^5. There is no direct comparison with values in the literature as the models are different. Indeed, in the same cavity but with variable ther-

modynamic properties of the fluid (Sutherland laws) LeQuéré *et al.* (1992) estimated a smaller critical Rayleigh number between 1.8×10^5 and 2×10^5. In a smaller cavity of aspect ratio 4, Weisman *et al.* (2001) estimated the transition at a larger value of Rayleigh between 3.2×10^5 and 3.4×10^5. In spite of these differences, the present value is nevertheless coherent since for example the larger confinement in the cavity of aspect ratio 4 stabilizes the flow.

The Rayleigh number has been again increased from 2.9×10^5 and the solution has remained oscillatory to $Ra = 3.4 \times 10^5$ (Figure 6) with a slight decrease of the period to 2.5. This value of Rayleigh number corresponds to the one previously investigated by Xin *et al.* (2002) in the BO approximation. The fluctuating temperature field (Figure 7-b) shows a similar pattern than those reported by LeQuéré *et al.* (1992) using Sutherland laws at $Ra = 2 \times 10^5$. Indeed, the field is made of 11 wavelengths (one wavelength being defined by two consecutives structures of alternative sign) of variable length which travel around the cavity in the direction of the primary circulation. The maximum amplitude of the fluctuating temperature is reached along the vertical side walls within the upper (lower) part along the hot (cold) wall like in boundary layer type instabilities. As already mentioned by LeQuéré *et al.* (1992), this solution at large value of ε, $\varepsilon = 0.6$, becomes strongly dissymmetric due to compressibility effects. The solution shows that fluctuations are almost constantly amplified along the hot wall and damped as they travel downward along the cold wall. Finally, one can also note that the thermal boundary layer is thicker than the velocity boundary layer as shown on the profiles in Figure 7-a.

The 2D finite amplitude time periodic solution obtained at $Ra = 3.4 \times 10^5$ has been interpolated in the third direction with 48 Fourier modes. This solution is shown to be unstable to an initial 3D perturbation. Indeed, the 2D solution becomes 3D, characterized by larger amplitudes of the velocity and a multi-frequencies spectrum (Figure 8).

The dominant frequencies are related to different modes of instability of Fourier wavenumbers in the range 1 to 14 (Figure 9). Over the computational time, the mode m=1 is globally dominant but the m=2 is able to become dominant during short time. The flow is characterized by the occurrence of large 3D structures in the x-direction under the form of elongated vortices in the z-direction (Figure 10).

By decreasing Rayleigh number step by step, the critical Rayleigh number Ra_c for convection was found to be twice weaker than in the 2D case at about $Ra = 1.4 \times 10^5$. Consequently, on contrary to the BO approximation the 2D solution is unstable to 3D perturbations, and natural convection at large temperature differences in 3D cavity is much more unstable than in the 2D one.

6. Conclusion

In this paper, a high order method has been proposed for solving three-dimensional equations in a low Mach number approximation. The numerical approach is carried

out with a spectral Chebyshev-Chebyshev-Fourier solver. Such approach is extended for the time to investigate natural convection with large temperature differences in closed cavity. The numerical code has been optimized on a vector computer and allows the investigation of 3D unsteady solutions. As an illustration, the 2D-3D transition has been studied in a tall differentially heated cavity of aspect ratio 8. On contrary to natural convection in Boussinesq convection where the transition to 3D does not occurred before being far from the onset of time dependence of 2D flow (Xin *et al.*, 2002), the 2D solutions here were found more unstable to 3D perturbations that suggest the 2D assumption is not valid for natural convection with large temperature difference in closed cavity.

Acknowledgment

The calculations were carried out on the NEC SX8 vector computer of the CNRS computational centre IDRIS.

7. References

Accary G., Raspo I., " A 3D finite volume method for the prediction of supercritical fluid buoyant flow in a differentially heated cavity", *Computer and Fluids*, vol. 35, p. 1316-1331, 2006.

Becker R., Braack M., " Solution of a stationary benchmark problem for natural convection with large temperature difference", *International Journal of Thermal Sciences*, vol. 41, p. 428-439, 2002.

Chenoweth D. R., Paolucci S., " Natural convection in an enclosed vertical air layer with large horizontal temperature differences", *Journal of Fluid Mechanics*, vol. 169, p. 173-210, 1986.

Christon M. A., Grecho P. M., Sutton S. B., " Computational predictability of time-dependent natural convection flows in enclosures (including a benchmark solution)", *International Journal for Numerical Methods in Fluids*, vol. 40, p. 953-980, 2002.

Fröhlich J., Peyret R., " Calculations of Non-Boussinesq Convection by a Pseudospectral Method", *Computer Methods in Applied Mechanics and Engineering*, vol. 80, p. 425-433, 1990.

Fröhlich J., Peyret R., " Direct spectral methods for the low Mach number equations", *International Journal of Numerical Methods for Heat and Fluid Flow*, vol. 2, p. 195-213, 1992.

Gauthier S., " A spectral collocation method for two dimensional compressible convection", *Journal of computational physics*, vol. 75, N°1, p. 217-235, 1988.

Gottlieb D., Orszag S. A., " Numerical analysis of spectral methods: Theory and applications", *SIAM, Philadelphia*, 1977.

Gray D. D., Giorgini A., " The Validity of the Boussinesq Approximation for Liquids and Gases", *International Journal of Heat and Mass Transfer*, vol. 19, p. 545-551, 1976.

Guo Y., Bathe K. J., " A numerical study of a natural convection flow in a cavity", *International Journal for Numerical Methods in Fluids*, vol. 40, p. 1045-1057, 2002.

Haidvogel D. B., Zang T. A., " The accurate solution of Poisson equation in Chebyshev polynomials", *Journal of computational physics*, vol. 30, p. 167-180, 1979.

Heuveline V., " On higher-order mixed FEM for low Mach number flows: application to a natural convection benchmark problem", *International Journal for Numerical Methods in Fluids*, vol. 41, p. 1339-1356, 2003.

Leong W. H., Hollands K. G. T., Brunger B. A., " On a physically realizable benchmark problem in internal natural convection", *International Journal of Heat and Mass Transfer*, vol. 41, p. 3817-3828, 1998.

LeQuéré P., Masson R., Perrot P., " A Chebyshev collocation algorithm for 2D non-Boussinesq convection", *Journal of computational physics*, vol. 103, p. 320-335, 1992.

LeQuéré P., Weismann C., Vierendeels H. P. J., Dicks E., et al. R. B., " Modelling of natural convection flows with large temperature differences: a benchmark problem for low Mach number solvers. Part1. Reference solutions", *Math. Model. Numer. Anal.*, vol. 39, p. 609-616, 2005.

Maday Y., Patera A. T., Ronquist E. M., " The $P_N \times P_{N-2}$ method for the approximation of the Stokes problem", *Laboratoire d'analyse numérique, Paris VI*, 1992.

Mohamad A. A., Bennacer R., Azaiez J., " Double diffusion natural convection in a rectangular enclosure filled with binary fluid saturated porous media; The effect of lateral aspect ratio", *Journal Physics of fluids*, vol. 16, p. 184-199, 2004.

Nicoud F., " Conservative high-order finite-difference schemes for low Mach number flows", *Journal of computational physics*, vol. 158, p. 71-97, 2000.

Paillere H., Viozat C., Kumbaro A., Toumi I., " Comparison of low Mach number models for natural convection problems", *Heat and Mass Transfer*, vol. 36, p. 567-573, 2000.

Paolucci S., " On the filtering of sound from the Navier-Stokes equations", *Technical report, Sandia National Laboratories USA*, 1982.

Roux B.*Note on Numerical Fluids Mechanics*, vol. 27, p. 227, 1990.

Saeid N. H., Mohamad A. A., " Natural convection in a square porous cavity with spatial Sidewall Temperature", *International journal for numerical methods for heat and fluid flow*, vol. 15, p. 555-566, 2005.

Vanel J. M., Peyret R., Bontoux P., " A pseudo-spectral solution of vorticity-stream function equations using the influence matrix technique", *Numerical methods for fluid dynamics II*, vol. , p. 463-475, 1986.

Weisman C., Calsyn L., Dubois C., LeQuéré P., " Sur la nature de la transition à l'instationnaire d'un écoulement de convection naturelle en cavité différentiellement chauffée à grands écarts de température", *Compte Rendu de l'Académie des Sciences*, vol. 329, Série II b, p. 343-350, 2001.

Xin S., LeQuéré P., " An extended Chebyshev pseudo-spectral benchmark for the 8:1 differentially heated cavity", *International journal for numerical methods in fluids*, vol. 40, p. 981-998, 2002.

Received: 17 April 2008
Accepted: 5 January 2009